

A Sliding Mode Controller of Hips Actuated for Passive Walking Robots

Sina Bakhtiari ^a, Mahdi Razzaghi ^b, Ahmad Samiee ^{c,*}

^a Mechanical Engineering Department, Islamic Azad University Tehran North Branch, Tehran, Iran

^b Management Engineering Department, Azad University Science and Research Branch, Tehran, Iran

^c Mechanical Engineering Department, Azad University Science and Research Branch, Tehran, Iran

Received 07 June 2019; Revised 07 August 2019; Accepted 04 November 2019; Available online 13 January 2020

Abstract

This paper addresses the application of using pneumatic force actuators at the hips of a five-link robotic system to provide a controllable input torque. The goal of this research is to provide a base to build upon to eventually produce an "active" biped walking robot that utilizes the benefits of the passive walking cycle. A reduced-order mathematical model of the system consisting of the pneumatic proportional valve and actuators is utilized in designing the force controller. The model takes into account tube links, valve friction, piston friction, and valve mechanics. The five-link robot is also modeled, including moments of inertia, masses, and centers of mass to design the trajectory controller. The mathematical models provide the equations necessary to develop the nonlinear control laws based on Sliding Mode Control Theory for both the force and trajectory controller. The controllers receive input signals from both pressure and position sensors located at the hips and position sensors at the knees. These signals are then converted into digital signals and processed by the computer using numerical analysis to obtain ethical values. Once the signals are input into the controllers, the experimental results of the actual system track the desired force and position trajectories defined for each controller within desired limits.

Keywords: *Biped walking robot, Pneumatic, Sliding Mode Control.*

1. Introduction

The dynamics of robots involves nonlinearities and intermittent collisions with the walking surface. Thus, the controllers that regulate their motions should be able to handle nonlinearities and intermittent actions. Many nonlinear control approaches have been proposed to control different applications. These include optimal control [1, 2], robust control [3,4], adaptive control [5,6], fuzzy control [7], and sliding mode control [8-9].

The motivation for designing hip actuated controllers for passive walking robots stems from the ongoing research in this area. Mochon and McMahon (1980) first introduced the idea of "ballistic walking" defined as a bipedal robot that does not require joint actuation during all phases of its gait. With this idea in mind, McGeer [10] proposed the concept of the "passive walker", which consisted of free joints without any actuation powered only by gravity. McGeer developed a mathematical model for describing the motion

* Corresponding author. Email: ahmad.samiee@srbiau.ac.ir

of passive walkers and built a two-dimensional robot based on this model. The significant advantages of passive walkers are their mechanical simplicity as well as their relatively high efficiency compared with active robots. McGeer studied a two-link robot with a hip mass that he demonstrated could walk down a shallow slope without any control. Later McGeer [11] introduced knees to his walking model, providing a passive means for foot clearance that is efficient and reliable. Camp [12] demonstrated that an open-loop control scheme could produce a stable powered walking cycle. His model replaced the energy loss to heel strike and friction by extending the leg powered by a permanent magnet DC motor at a constant voltage. He was able to produce stable gaits over a wide range of control parameters, which behaved similarly to previous passive walkers. Coleman and Ruina [13] built a two-legged toy that could walk. The toy could not balance statically, introducing the idea that uncontrolled non-holonomic mechanics may contribute to side-to-side balance.

Garcia et al. [14] produced computer simulations to create analytical methods to study the passive dynamics of the two-dimensional walkers first considered by McGeer. Their simplest 2-D model produced a short-step gait that is stable at small slopes and a long-step gait that exhibits period-doubling bifurcations, which leads to chaotic gait by varying the slope. Van der Linde [15] showed that smooth hip trajectories could be obtained by regulating leg stiffness and leg damping, creating a physically activated walker with new periodic gaits. The idea consisted of three muscle pairs excited by reflex-like trigger signals, which demonstrated that gait parameters like walking speed and step frequency could be manipulated by adjusting muscle or activation parameters [16]. Spong et al. [17] used potential energy shaping for compass gait bipeds to produce passive limit cycles that were slope invariant. He also addressed the use of switching control and its effect on the walker's sensitivity to initial conditions and its robustness to disturbance. Goswami et al. [18] studied compass gait walkers focusing on the stability and the periodicity properties of the passive motion. Their work showed that the introduction of a simple control scheme with only one control input could significantly increase the basin of attraction of the limit cycle for the bipedal gait. Kuo [19] studied a three-dimensional walker with a planar motion that allows for side-to-side tilting or roll. He discovered that passive cycles do exist for this model. However, the roll motion is unstable. Several

methods for stabilization were considered including direct and indirect control with the conclusion that quasi-static control of step width provides a simple and efficient solution to the problem.

Wisse et al. [20] introduced a three-dimensional biped to compensate for both yaw and roll. The model used a pelvic body as a passive dynamic compensator to take care of the yaw and roll motion while allowing the robot to move as a two-dimensional machine. Collins et al. [21] further studied three-dimensional passive walking robots with the development of an efficient kneed walker that used 1.3 W while walking and was able to compensate for both side-to-side lean and yaw with counter-swinging arms.

Also, Nikkhah et al. [22] presented a robust sliding mode tracking control scheme for an underactuated five-link planar robot with four actuators located at hip and knee joints. They showed the tracking stability of the biped's multistep walk by several numerical simulations. Besides, many other researchers studied different controllers on biped robots. Rahimi et al. [23] proposed an adaptive neural network sliding mode controller on a biped robot. They used a bat algorithm and showed effectiveness through numerical simulation. Taherkhorsandi et al. [24] presented a sliding mode control optimized by multi-objective genetic algorithm optimization to control a biped robot walking in the lateral plane on a slope. Here, we present a sliding mode controller on an experimental five-link biped robot. This robot is mounted by pneumatic actuators. To the best of our knowledge, it can be the novelty of this study.

This paper develops a method to provide the desired torque to the hip joint of a five-link robot using pneumatic actuators. To produce the desired torque using pneumatic actuators, a control scheme must be utilized that allows the control of the force generated by the actuators. Then a trajectory controller must be designed that defines the desired torque necessary to achieve the desired trajectory that is then converted to the desired force using the geometry of the system. The desired force can then be feed into the force controller. Both controllers used by the working robot are based on Sliding Mode theory as presented by Slotine and Li [25].

2. Model Development

In this section, we present the model with its details. At first, the two-link pneumatic system is described. Then, the

trajectory controller and implementation of the force controller are explained.

2.1. Description of a Two-Link Pneumatic System

The purpose of this paper is to demonstrate the feasibility of designing a pneumatic actuator to produce the desired torque at the hip joint, which can be adapted to passive walking robots. Since the actuators at the hip on each leg of the robot are symmetric only one leg of Fig. 1 consisting of two links an upper and lower leg connected to the hip will be considered in controller design. Once the pneumatic trajectory controller works for one joint, it can then be applied to other joints of the robot as needed.

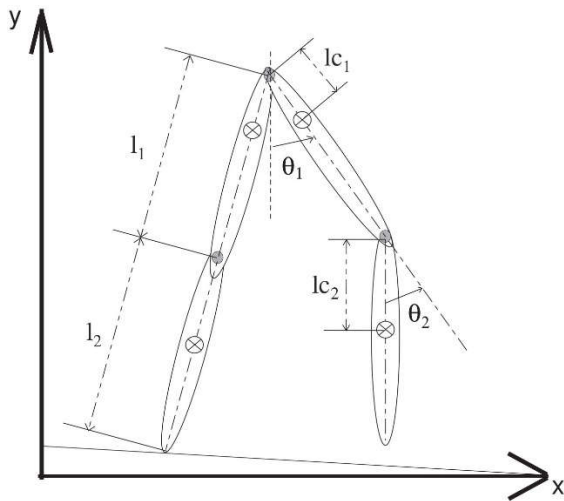


Fig. 1. Four-link passive walking model.

The system model for the trajectory controller includes two links consisting of an upper and lower leg with a knee joint connected to the hip. The model takes into account the parameters of the links such as the mass, center of mass, lengths, and moments of inertia. The system for the force controller consists of the Airpel actuator, connecting tubing, and proportional valve (see Fig. 2), which connects to the hip and upper leg of the two link robot. In order to obtain accurate results, detailed knowledge of the proportional valve must be available, including valve geometry, spring constants, and valve spool mass. The derivation of the force controller accounts for piston friction but assumes that there is no time delay for the pressure to propagate through the connecting tubing to the piston chambers. The values used

in the design and numerical testing of the controllers can be seen in Table 1.

2.2. Development of Trajectory Controller

The trajectory tracking controller was designed using the invariant structure control or Sliding Mode theory developed by Slotine and Li [31]. This type of controller was chosen because of its inherent properties of robustness to disturbances and model imprecisions. The equations of motion defining the two link system can be defined as follows:

$$M(q)\ddot{q} + C(q, \dot{q})\dot{q} + G(q) = \tau \quad (1)$$

where $M(q)$ is the mass matrix, $C(q, \dot{q})$ is the Coriolis matrix, $G(q)$ is the gravitational matrix, and τ is the input torque matrix with q defined as:

$$q = \begin{pmatrix} \theta_1 \\ \theta_2 \end{pmatrix} \quad (2)$$

where θ_1 and θ_2 correspond to the angles of the upper and lower legs, respectively, as seen in Fig. 1. The mass matrix is defined as:

$$M(q) = \begin{pmatrix} M_{11} & M_{12} \\ M_{21} & M_{22} \end{pmatrix} \quad (3)$$

$$M_{11} = \frac{1}{2} (2I_1 + 2l_{c1}^2 m_1 + l_1^2 m_2 + l_2^2 m_2 \quad (4)$$

$$+ 2l_{c2}^2 m_2 + (l_1^2 - l_2^2) m_2 \cos(2\theta_1)$$

$$+ 2(l_1 + l_2) l_{c2} m_2 \cos(\theta_2)$$

$$+ 2(l_1 - l_2) l_{c2} m_2 \cos(2\theta_1 + \theta_2))$$

$$M_{12} = M_{21} = \frac{1}{2} l_{c2} m_2 (2l_{c2} + (l_1 + l_2) \cos(\theta_1) \quad (5)$$

$$+ (l_1 - l_2) \cos(2\theta_1 + \theta_2))$$

$$M_{22} = I_2 + 2l_{c2}^2 m_2 \quad (6)$$

The Coriolis matrix is defined as:

$$C(q) = \begin{pmatrix} C_{11} & C_{12} \\ C_{21} & C_{22} \end{pmatrix} \quad (7)$$

$$C_{11} = -\frac{1}{2} m_2 \left((l_1 - l_2) ((l_1 + l_2) \sin(2\theta_1) \quad (8)$$

$$+ 2l_{c2} \sin(2\theta_1 + \theta_2)) \dot{\theta}_1$$

$$\begin{aligned}
& +(l_{c2}((l_1 + l_2) \sin(\theta_2) \\
& +(l_1 - l_2) \sin(2\theta_1 + \theta_2)))\dot{\theta}_2) \\
C_{12} = & -\frac{1}{2}l_{c2}m_2((l_1 + l_2) \sin(\theta_2) \\
& +(l_1 - l_2) \sin(2\theta_1 + \theta_2))(\dot{\theta}_1 + \dot{\theta}_2)
\end{aligned} \quad (9)$$

$$\begin{aligned}
C_{21} = & l_{c2}m_2(-l_1 \cos(\theta_1 + \theta_2) \sin(\theta_1) \\
& + l_2 \cos(\theta_1) \sin(\theta_1 + \theta_2))
\end{aligned} \quad (10)$$

$$C_{22} = 0 \quad (11)$$

And the gravitational matrix is defined as:

$$G(q) = \begin{pmatrix} G_1 \\ G_2 \end{pmatrix} \quad (12)$$

$$G_1 = g((l_{c1}m_1 + l_2m_2) \sin(\theta_1) + l_{c2}m_2 \sin(\theta_1 + \theta_2)) \quad (13)$$

$$G_2 = gl_{c2}m_2 \sin(\theta_1 + \theta_2) \quad (14)$$

Since this is an under-actuated system due to the fact that the only torque input is at the hip, the equations must be modified in order to derive a control law that can achieve trajectory tracking of the upper leg. This can be done by solving the second equation of motion from Eq. (1) for $\ddot{\theta}_2$ and substituting the result into the first equation of motion. This will lead to the following result:

$$\tilde{M}(\theta_1, \theta_2)\ddot{\theta}_1 + \tilde{C}(\theta_1, \theta_2, \dot{\theta}_1, \dot{\theta}_2)\dot{\theta}_1 + \tilde{G} = \tau \quad (15)$$

with

$$\tilde{M}(\theta_1, \theta_2) = M_{11} - \frac{M_{12}^2}{M_{22}} \quad (16)$$

$$\tilde{C}(\theta_1, \theta_2, \dot{\theta}_1, \dot{\theta}_2) = C_{11} - \frac{M_{12}C_{21}}{M_{22}} \quad (17)$$

$$\begin{aligned}
& -\frac{1}{2}m_2l_{c2}((l_1 + l_2) \sin(\theta_2) \\
& +(l_1 - l_2) \sin(2\theta_1 + \theta_2)) \\
\tilde{G} = & G_1 - \frac{M_{12}G_2}{M_{22}} + \frac{1}{2}m_2l_{c2}((l_1 + l_2) \sin(\theta_2) \\
& +(l_1 - l_2) \sin(2\theta_1 + \theta_2))\dot{\theta}_2
\end{aligned} \quad (18)$$

With the equations of motion-defined in this manner it is now possible to derive the desired control law. The scalar s will be:

$$s = \dot{\theta}_1 - \dot{\theta}_{1r} \quad (19)$$

$$\dot{\theta}_{1r} = \dot{\theta}_{1d} - \lambda(\theta_1 - \theta_{1d}) \quad (20)$$

where θ_{1d} is the desired trajectory for the upper link. With s defined, it is possible to define a Lyapunov function for the system such that:

$$V = \frac{1}{2}\tilde{M}(\theta_1, \theta_2)s^2 \quad (21)$$

By using Eq.(15) and setting the time derivative of Eq.(21) equal to zero, the desired control torque ($\hat{\tau}$) necessary for tracking can be computed, which would control the system assuming the dynamics are precisely known. From this, the control input can be defined as:

$$\tau = \hat{\tau} + K \operatorname{sgn}(s) \quad (22)$$

where $\operatorname{sgn}(s)$ is the sign function on variable s and the gain K is defined in such a way to guarantee that the surface $s=0$ is reached in a finite amount of time according to the following:

$$K \geq |\tilde{M}\ddot{\theta}_{1r} + \tilde{C}\dot{\theta}_{1r} + \tilde{G}| + \eta \quad (23)$$

with η chosen as a strictly positive number to satisfy the sliding condition. The $\operatorname{sgn}(s)$ function in Eq.(22) introduces a switching function into the gain of the controller, which would result in mechanical chattering in the physical model. One solution to this problem consists of replacing the $\operatorname{sgn}(s)$ function with a saturation function ($\operatorname{sat}(s)$) that smooths the function producing a gain as follows:

$$\tau = \hat{\tau} + K\operatorname{sat}\left(\frac{s}{\Phi}\right) \quad (24)$$

Where the $\operatorname{sat}\left(\frac{s}{\Phi}\right)$ function is written as:

$$\operatorname{sat}\left(\frac{s(t)}{\Phi}\right) = \begin{cases} \frac{s(t)}{\Phi} & \left|\frac{s(t)}{\Phi}\right| < 1 \\ \operatorname{sgn}(s(t)) & \left|\frac{s(t)}{\Phi}\right| \geq 1 \end{cases} \quad (25)$$

And Φ is the thickness of a thin boundary layer around the switching function.

We used numerical simulation to test the validity of the trajectory controller to ensure tracking would be within acceptable tolerances for the parameters previously listed in Table1. The uncertainties assumed in the mass, Coriolis, and

gravitational matrices to test the robustness of the controller were as follows:

$$\hat{M} = \tilde{M} - 0.1\tilde{M} \quad (26)$$

$$\hat{C} = \tilde{C} - 0.2\tilde{C} \quad (27)$$

$$\hat{G} = \tilde{G} - 0.1\tilde{G} \quad (28)$$

Table 1: Physical parameters of the system

	Parameter	Value
Upper Leg	l_1	0.408 m
	m_1	0.67 Kg
	l_{c1}	0.1523 m
	I_1	0.0108 Kg.m ²
Lower Leg	l_2	0.4195 m
	m_2	0.22 Kg
	l_{c2}	0.24 m
	I_2	0.0053 Kg.m ²

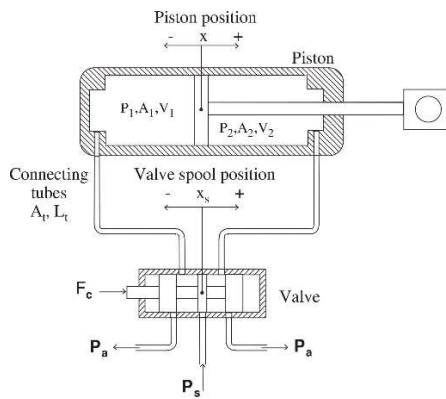


Fig. 2. Representation of the pneumatic system.

The sampling rate chosen to test the controller was taken to be 1000 samples/second since that corresponded with the capabilities of the equipment to be used in the experimental setup. The simulation shows that relatively small torques are required at the hip to achieve the desired tracking, as seen in Fig. 3. Figures 4-6 confirm that the controller behaves appropriately during simulation tracking the desired sine function with relatively small error.

2.3. Implementation of Force Controller

Once the trajectory controller calculates the desired torque needed, then this value must be feed into the force controller. The trajectory controller defines the necessary torque required to achieve the desired trajectory; however, the force controller needs the desired force as an input. In order to convert the desired torque into the desired force the geometry of the actuator connection from the hip to the upper leg must be taken into account. A lever arm extruding from the hip is used to connect the actuator from the upper leg to the hip in such a way that the force created by the piston will generate a torque about the hip as seen in Fig. 7. The desired force can be calculated using the following relationship:

$$F_d = \frac{\tau c(t)}{a b \sin(\gamma - \theta_1)} \quad (29)$$

Where γ is a constant angle concerning the vertical, and the length $c(t)$ is determined by the position of the piston. The force controller controls the valve spool, which allows for the control of the pressures on each side of the piston, making it possible to produce the desired force. By neglecting valve dynamics and the time delay introduced by the connecting tubes, the pneumatic system is reduced to a first-order system with a scalar s as:

$$s = P_1 A_1 - P_2 A_2 - P_a A_r - \beta \dot{x} - F_d \quad (30)$$

With P_1 and P_2 corresponding to the pressures in each chamber of the piston (see Fig. 2), and A_1 and A_2 refer to the area of the piston the pressures are acting upon. A friction coefficient for the piston is represented by β . Differentiating s reveals the dynamics of the sliding mode as:

$$\dot{s} = \dot{P}_1 A_1 - \dot{P}_2 A_2 - \beta \ddot{x} - \dot{F}_d \quad (31)$$

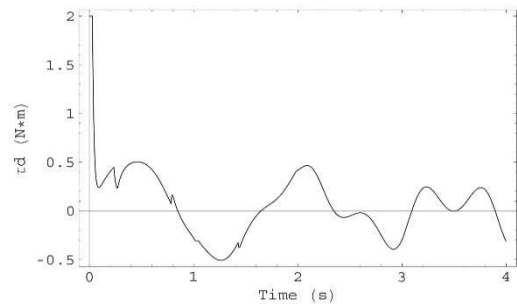


Fig. 3. Torque required for trajectory tracking in the numerical simulation.

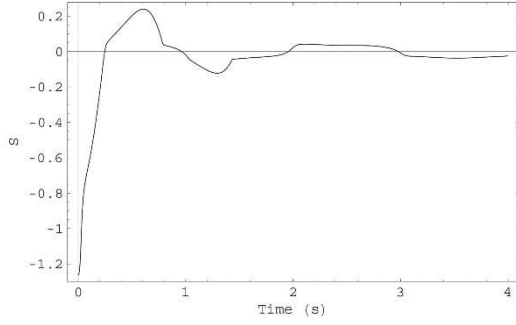
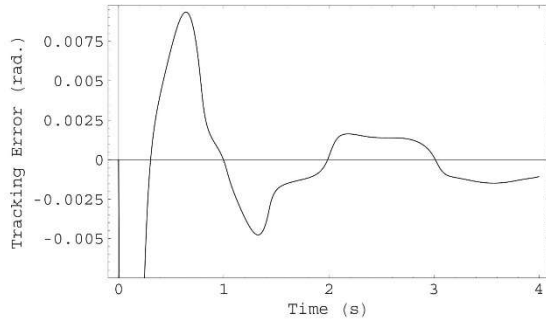
Fig. 4. Scalar s for the numerical simulation.

Fig. 5. Trajectory error of the numerical simulation.

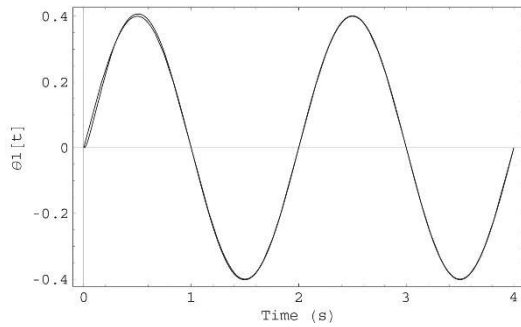


Fig. 6. Trajectory tracking of the numerical simulation.

By substituting in the appropriate values for the pressure derivatives which are not derived here, the time derivative of scalar s becomes:

$$\begin{aligned} \dot{s} = & A_{v_{in}} K_f \left(\frac{A_1 P_s \alpha_{in} \phi_{in} \dot{m}_r(P_s, P_1)}{V_1} \right. \\ & + \frac{A_2 P_2 \alpha_{ex} \phi_{ex} \dot{m}_r(P_2, P_a)}{V_2} \\ & - A_{v_{ex}} K_f \left(\frac{A_1 P_1 \alpha_{ex} \phi_{ex} \dot{m}_r(P_1, P_a)}{V_1} \right. \\ & + \frac{A_2 P_s \alpha_{in} \phi_{in} \dot{m}_r(P_s, P_2)}{V_2} \left. \right) \alpha \left(\frac{A_1^2 P_1}{V_1} + \frac{A_2^2 P_2}{V_2} \right) \dot{x} \\ & - \beta \ddot{x} - \dot{F}_d = 0 \end{aligned} \quad (32)$$

where $A_{v_{in}}$ is the input flow valve area, $A_{v_{ex}}$ is the exhaust flow valve area, P_s is the supply pressure, P_a is the ambient pressure, the terms α are the corresponding heat transfer coefficients, and V_1 and V_2 represent the volumes associated with each side of the actuator piston. The connecting tube attenuation function ϕ is defined as:

$$\phi = e^{\frac{-32\mu R T L_t}{2c P D^2}} \quad (33)$$

where μ represents the dynamic viscosity of air, R is the ideal gas constant, T is the temperature of the gas, L_t is the length of the corresponding tube, c is the speed of sound, P is the associated pressure for that tube, and D refers to the inner diameter of the corresponding tube. The reduced mass flow function defined as:

$$\dot{m}_r = \begin{cases} C_f C_1 \frac{P_u}{\sqrt{T}} & \frac{P_d}{P_u} \leq P_{cr} \\ C_f C_1 \frac{P_u}{\sqrt{T}} \left(\frac{P_d}{P_u} \right)^{\frac{1}{k}} \sqrt{1 - \left(\frac{P_d}{P_u} \right)^{k - \frac{1}{k}}} & \frac{P_d}{P_u} > P_{cr} \end{cases} \quad (34)$$

with C_1 as the flow constant for the given fluid, C_f as the discharge coefficient, P_u and P_d as the pressure upstream and downstream respectively, and P_{cr} as the critical pressure ratio completes the functions necessary to define the appropriate dynamics of the sliding surface.

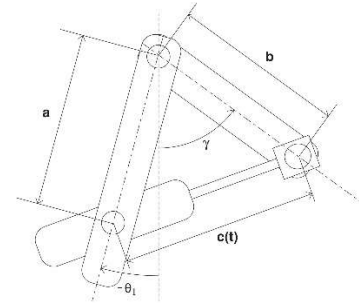


Fig. 7. Actuator Geometry.

Due to the physical characteristics of the valve air paths, the input and exhaust cannot both be nonzero at the same time. This leads to two cases, one when $s < 0$ leading to:

$$A_{v_{in}} = \frac{V_1 V_2 \left(\beta \ddot{x} + \dot{F}_d - K_v \text{sat} \left(\frac{\dot{s}}{\Phi} \right) \right) + \alpha (V_2 A_1^2 P_1 + V_1 A_2^2 P_2) \dot{x}}{K_f (V_2 A_1 P_s \alpha_{in} \phi_{in} \dot{m}_r(P_s, P_1) + V_1 A_2 P_2 \alpha_{ex} \phi_{ex} \dot{m}_r(P_2, P_a))} \quad (35)$$

$$A_{v_{ex}} = 0 \quad (36)$$

and the second when $s > 0$ causing

$$A_{v_{in}} = 0 \tag{37}$$

$$A_{v_{ex}} = -\frac{V_1 V_2 \left(\beta \ddot{x} + \dot{F}_d - K_v \text{sat}\left(\frac{\dot{s}}{\Phi}\right) \right) + \alpha (V_2 A_1^2 P_1 + V_1 A_2^2 P_2) \dot{x}}{K_f (V_2 A_1 P_1 \alpha_{ex} \phi_{ex} \dot{m}_r(P_1, P_a) + V_1 A_2 P_2 \alpha_{in} \phi_{in} \dot{m}_r(P_2, P_2))} \tag{38}$$

where $K_v \text{sat}\left(\frac{\dot{s}}{\Phi}\right)$ term is added to this equation to compensate for imprecision in the model in order to effect \dot{s} directly. Both K_v and Φ are chosen as constants to simplify the controller design.

3. Experimental Results

The next challenge after producing a numerical model that demonstrated the expected behavior of the controllers in providing the desired trajectory was to build a physical robot that behaved similarly. The robot parameters for the physical model were chosen to approximate the values used in the numerical simulation shown in Table 1. The complete physical model consisted of a four-link robot made out of Maytec aluminium profiles, two pneumatic valves, two Airlpel actuators, connecting tubing, a computer, and electronics connecting the valve to the computer. Figure 8 shows a picture of the physical model and the location of the valves, actuators, and electronics.

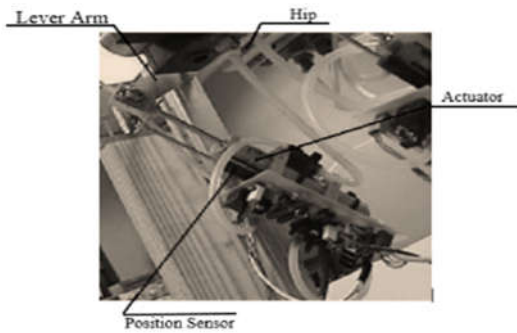


Fig. 8. Actuator geometry of the physical system.

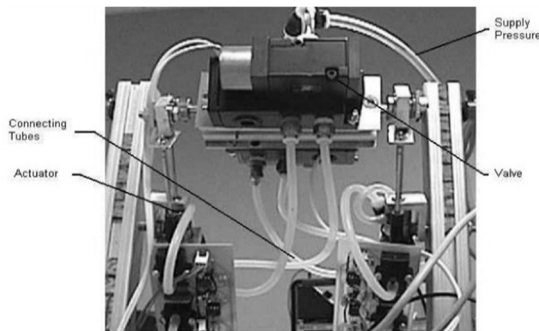


Fig. 9. Pneumatic setup of the physical system.

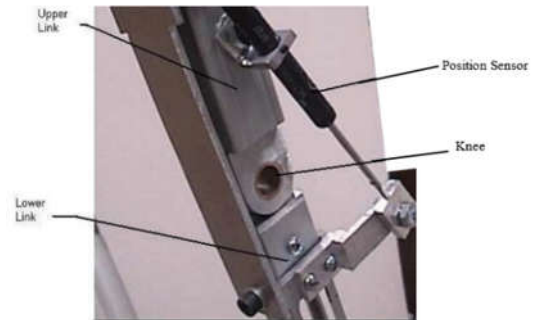


Fig. 10. Knee geometry for measuring θ_2 .

The first step in building the physical model consisted of determining how the torque would be applied to the hip joint. Since actuators would be used to create a force, a lever arm extending from the hip was needed to convert the force created into a torque. Figure 9 shows how this was done, giving a side view of the actuator and lever arm about the hip joint. The pneumatic system for the physical model is seen in Fig. 9, which shows the position of the valves connected to the hip as well as the location of the actuators and connecting tubing. In order to obtain the information necessary for the controllers, pressure sensors for each side of the piston were implemented to achieve the pressure readings needed. Position sensors for both the piston position, which was also used to calculate θ_1 and the angle of the second link (θ_2) were required by the controller. It can be seen from Fig. 8 how the position sensor for θ_1 was mounted in parallel with the actuator to obtain the piston position. Similarly, a second position sensor was installed around the knee to measure, θ_2 as seen in Fig. 10. The pressure sensors were mounted underneath the actuators on the circuit board to minimize the links of the tubes connecting the pressure sensors to the piston chambers to obtain the most accurate value possible.

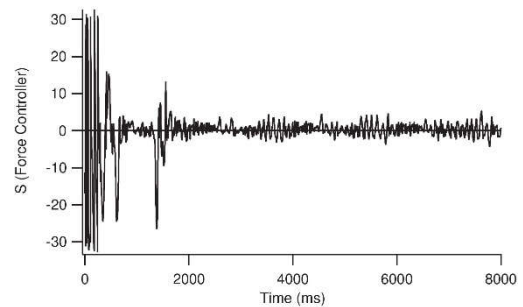


Fig. 11. Scalar s for force controller average walking speed.

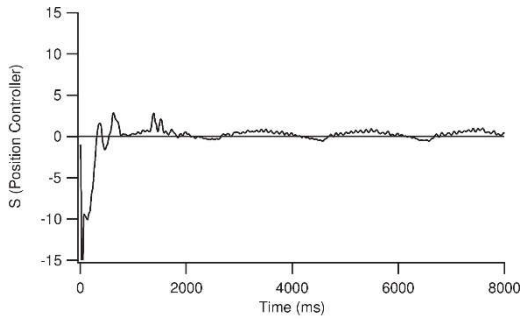


Fig. 12. Scalar s for trajectory controller average walking speed.

The controllers developed in Section 2 were coded into the computer using C++ programming using a custom command for the Arduino. All sensor information was fed into the computer through the Arduino. With this information, the controllers have all the information required for the control laws to be applied to the physical system. The output current needed to control the valve is then created through the output on the data acquisition card and a simple circuit to convert the voltage supplied by the card into the appropriate current. To test the physical model, three different frequencies were chosen over the range of various walks. The first trajectory used corresponds to a stroll, the second to an average walking speed, and the third to a brisk walk. The desired equations corresponding to these trajectories are as follows, respectively.

$$\theta_{1d} = -0.3 \sin(0.5\pi t) \quad (39)$$

$$\theta_{1d} = -0.3 \sin(\pi t) \quad (40)$$

$$\theta_{1d} = -0.3 \sin(2\pi t) \quad (41)$$

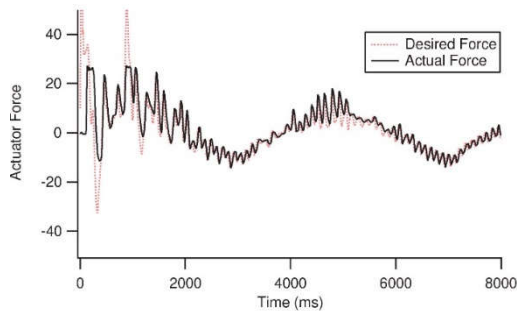


Fig. 13. Force tracking of the controller for the slow stroll.

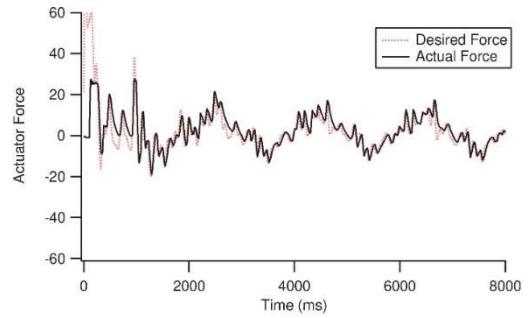


Fig. 14. Force tracking of the controller for the average walk.

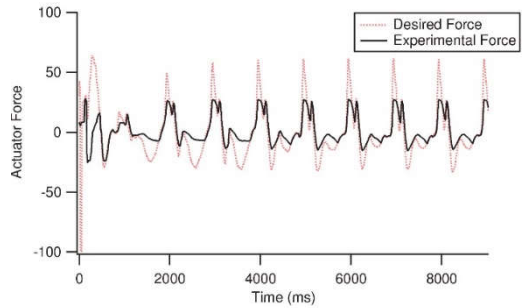


Fig. 15. Force tracking of the controller for the brisk walk.

The amplitude of the sine functions used correspond closely to the angles of the stance and swing legs for the passive models studied by McGeer. Based on testing of the physical model and the calibration of the control parameters to ensure that the force and trajectory controllers were tracking the following results were produced. Figures 11 and 12 show that the scalar s for both the force and trajectory controllers die off in a finite amount of time and is only shown for the average walking speed.

Next, the performance of the force controller as well as the trajectory controller was evaluated to determine the effects the controllers might encounter within the range of walking speeds defined above. For the slow stroll and the average walking speeds, the force controller is able to track the desired force with very little error within the first two seconds, as seen in Fig. 13 and 14. The force tracking for the brisk walking speed displayed in Fig. 17, however, does not track near as well. This appears to be caused by the knee stop used to prevent the lower leg from bending the wrong direction. When the lower leg causes the knee stop to hit the upper leg, the impact produces a force on the upper leg, which is not modeled in the equations of motion.

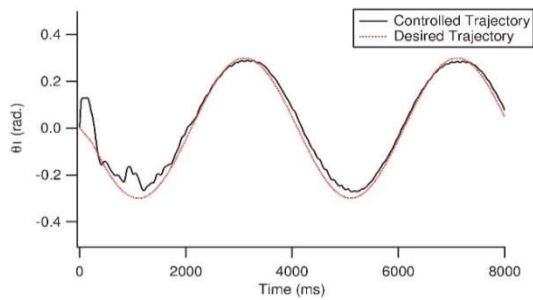


Fig. 16. Trajectory tracking of the controller for the slow stroll.

Under lower walking speeds this disturbance does not significantly affect the performance of the controller, however, at higher velocities the force with which the knee stop impacts the upper leg increases to the point the sliding mode controller can no longer compensate for the disturbance. As expected since the force controller is tracking well for the slow and average walking speeds, their trajectories follow their corresponding desired trajectories very closely, as seen in Fig. 16 and 17. On closer inspection of these figures, one can notice that the controller tracks the positive peak of the desired trajectory better than the negative peak. This phenomenon also appears to be related to the knee stop. Since at this point on the graph the leg is in the locked or straight position with the knee stop preventing the lower leg from hyperextending, the upper and lower leg is acting more like a single link system instead of the two link system used to design the controller. The trajectory tracking for the brisk walking speed in Fig. 18 does not follow the desired path as closely as the other two walking speeds. The main reason for this is the fact that the force controller is not able to produce the desired forces needed to counteract the discontinuous nature of the knee stop impact at this speed. Through observation, the knee stop impacting the upper leg for the brisk walk occurs when the trajectory deviates from the desired trajectory and then overcompensates and overshoots the desired trajectory.

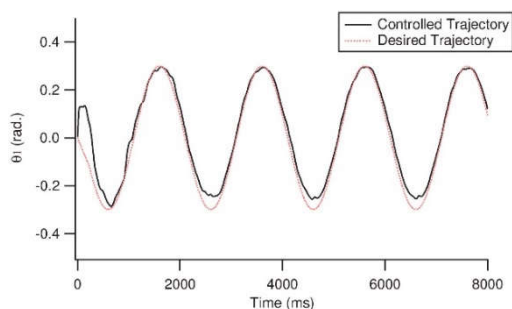


Fig. 17. Trajectory tracking of the controller for the average walk.

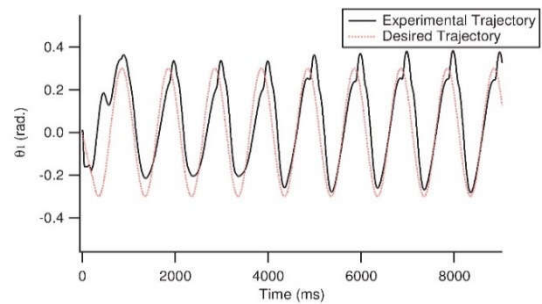


Fig. 18. Trajectory tracking of the controller for the brisk walk.

4. Conclusion

In this paper, we described a mathematical model to design and test the feasibility of producing a hip actuated controller. The model takes into account the physics of the robotic links and the dynamics of the pneumatic valve and piston, including attenuation caused by the connecting tubes. Through numerical testing, the proposed model demonstrates that a pneumatic force controller in conjunction with a trajectory controller is sufficient to control the trajectory for most walking speeds. Due to the highly nonlinear characteristics and uncertainties in the pneumatic systems sliding mode control theory was implemented in both controllers. Using this control scheme insures that the system will be robust regarding the sensitivity of initial conditions and unwanted disturbances. The reduced order force controller was chosen since the desired results could be achieved using the simpler control scheme. It should be noted that this controller may not work as well if connecting tubes are relatively long or if the frequency of the desired force exceeds 25 Hz.

Both controllers were designed and implemented on a four-link robot. Two sets of controllers were used, one for each leg of the robot producing the desired trajectory for both upper legs within acceptable tolerances. One leg was given a sine function to follow while simultaneously the other leg was following a minus sine function to give the appearance of a robot walking. The controllers demonstrated only slight attenuation at the peaks with the control parameters and numerical processing used to achieve tracking for the slow stroll and average walking speeds. The desired tracking for fast walking speeds, however, did not track quite as well. Future work related to this project would include inputting a passive gait trajectory into the controller to produce an active walker. This would take advantage of the inherent properties of passive walkers.

References

- [1] Razzaghi, P.; Assadian, N., "Study of the triple-mass tethered satellite system under aerodynamic drag and j_2 perturbations", *Advances in Space Research*, vol. 56, no. 10, pp. 2141–2150 (2015).
- [2] Razzaghi, P.; Al Khatib, E.; Bakhtiari, S., "Sliding mode and SDRE control laws on a tethered satellite system to de-orbit space debris", *Advances in Space Research*, vol. 64, no. 1, pp. 18–27 (2019).
- [3] Khiabani, A. G.; Babazadeh, R., "Design of robust fractional-order lead-lag controller for uncertain systems", *IET Control Theory & Applications*, vol. 10, no. 18, pp. 2447–2455 (2016).
- [4] Navabi, M.; Mirzaei, H., "Robust optimal adaptive trajectory tracking control of quadrotor helicopter", *Latin American Journal of Solids and Structures*, vol. 14, no. 6, pp. 1040–1063 (2017).
- [5] Navabi, M.; Mirzaei, H., "0d based nonlinear tracking control of quadcopter", in 2016 4th International Conference on Robotics and Mechatronics (ICROM). IEEE, pp. 331–336 (2016).
- [6] Al Khatib, E. I.; Al-Masri, W. M.; Mukhopadhyay, S.; Jaradat, M. A.; Abdel-Hafez, M., "A comparison of adaptive trajectory tracking controllers for wheeled mobile robots", in *Mechatronics and its Applications (ISMA), 2015 10th International Symposium on*. IEEE, pp. 1–6 (2015).
- [7] Al Khatib, E. I.; Jaradat, M. A.; Abdel-Hafez, M.; Roigari, M., "Multiple sensor fusion for mobile robot localization and navigation using the extended kalman filter", in *Mechatronics and its Applications (ISMA), 2015 10th International Symposium on*. IEEE, pp. 1–5 (2015).
- [8] Nateghi, S.; Shtessel, Y.; Barbot, J.-P.; Zheng, G.; Yu, L., "Cyber-attack reconstruction via sliding mode differentiation and sparse recovery algorithm: Electrical power networks application", in 2018 15th International Workshop on Variable Structure Systems (VSS). IEEE, pp. 285–290 (2018).
- [9] Nateghi, S.; Shtessel, Y.; Barbot, J.-P.; Edwards, C., "Cyber attack reconstruction of nonlinear systems via higher-order sliding-mode observer and sparse recovery algorithm", in 2018 IEEE Conference on Decision and Control (CDC). IEEE, 2018, pp. 5963–5968 (2018).
- [10] McGeer, T., "Passive dynamic walking", *International Journal of Robotic Research*, vol. 9, no. 2, pp. 62–82 (1990).
- [11] McGeer, T., "Passive walking with knees", in *Proceedings, IEEE International Conference on Robotics and Automation*, May 1990, vol. 3, pp. 1640–1645 (1990).
- [12] Camp, J., "Powered "passive" dynamic walking", *Masters of Engineering Project Report*, Cornell University (1997).
- [13] Coleman, M. J.; Ruina, A., "An uncontrolled walking toy that cannot stand still", *Physical Review Letters*, vol. 80, no. 16, pp. 3658–3661 (1998).
- [14] Garcia, M.; Chatterjee, A.; Ruina, A.; Coleman, M., "The simplest walking model: stability, complexity, and scaling", *Journal of biomechanical engineering*, vol. 120, no. 2, pp. 281–288 (1998).
- [15] Van Der Linde, R. Q., "Active leg compliance for passive walking", in *Proceedings. 1998 IEEE International Conference on Robotics and Automation (Cat. No. 98CH36146)*, vol. 3, pp. 2339–2344 (1998).
- [16] Van Der Linde, R. Q., "Passive bipedal walking with phasic muscle contraction", *Biological cybernetics*, vol. 81, no. 3, pp. 227–237 (1999).
- [17] Spong, M. W., "Passivity based control of the compass gait biped", in *Proc. of IFAC World Congress*, pp. 19–23 (1999).
- [18] Goswami, A.; Espiau, B.; Keramane, A., "Limit cycles and their stability in a passive bipedal gait", in *Proceedings of IEEE International Conference on Robotics and Automation*, vol. 1. IEEE, 1996, pp. 246–251 (1996).
- [19] Kuo, A. D., "Stabilization of lateral motion in passive dynamic walking", *The International journal of robotics research*, vol. 18, no. 9, pp. 917–930 (1999).
- [20] Wisse, M.; Schwab, A. L., "A 3d passive dynamic biped with yaw and roll compensation", *Robotica*, vol. 19, no. 3, pp. 275–284 (2001).
- [21] Collins, S. H.; Wisse, M.; Ruina, A., "A three-dimensional passive-dynamic walking robot with two legs and knees", *The International Journal of Robotics Research*, vol. 20, no. 7, pp. 607–615 (2001).
- [22] Nikkhah, M.; Ashrafiuon, H.; Fahimi, F., "Robust control of underactuated bipeds using sliding modes", *Robotica*, vol. 25, no. 3, pp. 367–374 (2007).
- [23] Rahmani, M.; Ghanbari, A.; Etefagh, M., "A novel adaptive neural network integral sliding-mode control of a biped robot using bat algorithm", *Journal of Vibration and Control*, vol. 24, no. 10, pp. 2045–2060 (2019).
- [24] Taherkhorsandi, M.; Mahmoodabadi, M. J.; Talebipour, M.; Castillo-Villar, K. K., "Pareto design of an adaptive robust hybrid of PID and sliding control for a biped robot via genetic algorithm optimization", *Nonlinear dynamics*, vol. 79, no. 1, pp. 251–263 (2015).
- [25] Slotine, J.-J. E.; Li, W., "Applied nonlinear control", Prentice hall Englewood Cliffs, NJ, vol. 199, no. 1 (1991).